











Vibrational and structural properties of the $R\text{Fe}_4\text{Sb}_{12}$ ($R = \text{Na}, \text{K}, \text{Ca}, \text{Sr}, \text{Ba}$) filled skutterudites

Juliana G. de Abrantes ^{1,*}, Marli R. Cantarino ¹, Wagner R. da Silva Neto ^{1,2}, Victória V. Freire ¹,
 Alvaro G. Figueiredo ¹, Tarsis M. Germano ¹, Bassim Mounssef, Jr. ², Eduardo M. Bittar ³,
 Andreas Leithe-Jasper ⁴ and Fernando A. Garcia ^{1,†}

¹Instituto de Física, Universidade de São Paulo, 05508-090, São Paulo-SP, Brazil

²Instituto de Química, Universidade de São Paulo, 05508-090, São Paulo-SP, Brazil

³Centro Brasileiro de Pesquisas Físicas, Rio de Janeiro, RJ 22290-180, Brazil

⁴Max Planck Institute for Chemical Physics of Solids, D-01187 Dresden, Germany



(Received 14 February 2022; revised 10 June 2022; accepted 8 July 2022; published 16 August 2022)

Vibrational and elastic properties of the $R\text{Fe}_4\text{Sb}_{12}$ skutterudites are investigated by, respectively, temperature (T) dependent extended x-ray absorption fine structure (EXAFS) and pressure (P) dependent x-ray diffraction (XRD) experiments. The Fe K -edge EXAFS experiments of the $R = \text{K}, \text{Ca}$, and Ba materials were performed in the T interval $6 < T < 300$ K and XRD experiments of the $R = \text{Na}, \text{K}, \text{Ca}, \text{Sr}$, and Ba materials were performed in the P interval $1 \text{ atm} < P < 16$ GPa. From EXAFS, we obtained the correlated Debye-Waller parameters that were thus analyzed to extract effective spring constants connected with the Fe- Y (where $Y = \text{either } R, \text{Fe or Sb}$) scattering paths. Our findings suggest that in the case of the light cations, $R = \text{K}$ or Ca , the R atoms are relatively weakly coupled to the cage, in a scenario reminiscent to the Einstein oscillators. From the XRD experiments, we obtained the bulk modulus B_0 for all $R = \text{Na}, \text{K}, \text{Ca}, \text{Sr}$, and Ba materials, with values ranging from 77 GPa ($R = \text{K}$) to $R = 99$ GPa ($R = \text{Ba}$) as well as the compressibility β as a function of P . The trend in β as a function of the R filler is discussed and it is shown that it does not correlate with simple geometrical considerations but rather with the filler-cage bonding properties.

DOI: [10.1103/PhysRevMaterials.6.085403](https://doi.org/10.1103/PhysRevMaterials.6.085403)

I. INTRODUCTION

Filled skutterudites are materials with chemical formula RT_4X_{12} where the T_4X_{12} elements form a relatively rigid cage framework inside which the R elements are allocated [1]. In the simplest chemical bonding scenario, the cage is structured by strong T - X covalent bondings and the R fillers generically display a cationic character, donating electrons that further stabilize the T_4X_{12} cage. While it is well known that the description of bonding in filled skutterudites is more involved [2], this simple picture can be applied as a guide to discover new filled skutterudites [3] as well as to justify their unusual vibrational dynamics [4].

Concerning the latter topic, research on the filled skutterudites is indeed triggered mostly by the presence of an unusual vibrational dynamics that makes the filled skutterudites good candidates for thermoelectric applications [5–7]. In this regard, earlier contributions proposed that the R fillers behave as independent, nondispersive, and low-energy oscillators (or rattlers), that scatter the cage derived phonons, giving rise to a phonon glass, which impedes the thermal conduction and raises the material thermoelectric figure of merit ZT [8].

On one account, the phonon glass scenario provided a first approach to understand the skutterudites' vibrational dynamics. For instance, filling the cages with distinct fillers may cause the smaller R cations to display an unusual rattling behavior in the oversized cage, as observed [9,10]. This

scenario, however, was soon challenged [11] and it is now well understood that the separation between rattler and cage vibrational dynamics does not offer an adequate description of the filled skutterudite vibrational properties [12–14]. All this understanding is particularly true in the case of the $R\text{Fe}_4\text{Sb}_{12}$ ($R = \text{Na}, \text{K}, \text{Ca}, \text{Sr}, \text{Ba}, \text{La}$, and Yb) skutterudites [15–20] and provides support for the design of more efficient antimony-based skutterudite materials [21–23].

On top of the good potential for thermoelectric applications, filled skutterudites are very flexible platforms, displaying a broad range of electronic, magnetic, and thermal properties [24]. The $R\text{Fe}_4\text{Sb}_{12}$ ($R = \text{Na}, \text{K}, \text{Ca}, \text{Sr}, \text{Ba}$, and La) materials, in particular, are itinerant magnets [15,25–29] whose magnetic properties are dominated by a high density of states due to the mixing between the Fe derived $3d$ states and Sb-derived $5p$ states forming heavy bands in the vicinity of the Fermi level [30,31].

In this work, we focus on the vibrational and structural properties of the $R\text{Fe}_4\text{Sb}_{12}$ ($R = \text{Na}, \text{K}, \text{Ca}, \text{Sr}$, and Ba) filled skutterudites as investigated, respectively, by temperature (T) dependent extended x-ray absorption fine structure (EXAFS) and pressure-dependent (P -dependent) x-ray diffraction (XRD) experiments. EXAFS was soon recognized by Cao *et al.* [32] as a suitable probe for the site-specific vibrational dynamics in skutterudites. Later contributions [33–35] developed the application of the technique to the correlated nature of the filler-cage vibrational dynamics. Here, we focus on the Fe K -edge EXAFS of the $R = \text{K}, \text{Ca}$, and Ba samples. In our investigation, we find that the cage vibrational dynamics clearly depends on the filler type, corroborating the correlated nature of the filler-cage dynamics.

*juliana.abrantes@usp.br

†fgarcia@if.usp.br

Our XRD experiments were carried out for pressures typically up to ≈ 16 GPa for all samples, except in the case of $\text{BaFe}_4\text{Sb}_{12}$, which was investigated up to 24 GPa. Overall, the P dependence of all samples is well described by the Birch-Murnaghan model [36] from which we extract the bulk modulus B_0 for each R . The B_0 behavior as a function of R is discussed in the context of bonding specific properties of the $R\text{Fe}_4\text{Sb}_{12}$ skutterudites. This discussion is supported by quantum chemistry calculations. Moreover, starting at pressures about ≈ 12 GPa, the XRD results display broad reflections. This finding suggests that the $R\text{Fe}_4\text{Sb}_{12}$ materials undergo a process of increasing lattice disorder triggered by pressure, which is reminiscent of the pressure-induced partial amorphization observed for other cage systems [37].

II. METHODS

High-quality polycrystalline samples of $R\text{Fe}_4\text{Sb}_{12}$ ($R = \text{Na}, \text{K}, \text{Ca}, \text{Sr}, \text{and Ba}$) skutterudites were synthesized by a solid-state sintering method [25]. Fe K -edge EXAFS experiments of the $R = \text{K}, \text{Ca}, \text{and Ba}$ samples were performed at the XAFS2 [38] beamline of the Brazilian Synchrotron Light Source (CNPEM-LNLS). The spectra of the K- and Ca-filled materials were measured by both fluorescence and transmission modes, whereas the Ba-filled material was measured only in the fluorescence mode. A complete temperature scan in the interval $300 > T > 6$ K was obtained for the three samples. An Fe foil, kept at room temperature, was measured in the transmission mode as a reference throughout the experiments. A conventional He-flow cryostat was employed to achieve temperatures down to $T = 6$ K.

The EXAFS data were analyzed by multiple-scattering theory implemented by the FEFF code [39]. The graphical Demeter platform [40] was adopted to perform the fittings of a structural model including single- and multiple-scattering paths up to 5 Å from the Fe absorber. To decrease the number of parameters in the fitting, the EXAFS S_0^2 parameter (the path amplitudes) was obtained from *ab initio* calculations implemented by the FEFF8.4 code. The *ab initio* calculations were performed for clusters of 226 atoms, adopting the Hedin-Lundqvist pseudopotential to account for the exchange interaction [31].

The powder XRD experiments were performed at the XDS [41] beamline of the CNPEM-LNLS at room temperature. A diamond-anvil cell (DAC) was employed during experiments to achieve pressures up to 24 GPa ($R = \text{Ba}$), but typically up to 16 GPa ($R = \text{Na}, \text{K}, \text{Ca}, \text{and Sr}$). A mixture of methanol and ethanol (in a 1 : 4 proportion) was adopted as a pressure media. The pressure was measured by monitoring the Raman fluorescence from a ruby standard mounted in the DAC together with the samples. In all measurements, the x-ray energy was set to 20 keV. The XRD powder profile fitting and background removal were performed with the GSAS-II software [42].

The filler-cage bonding properties of the $R = \text{Ca}, \text{Sr}, \text{and Ba}$ -filled materials were calculated within the density-functional theory (DFT) approximation, adopting the ORCA 5.0 program package [43,44]. A supercell containing a total of 339 atoms was generated for the calculations which were implemented in an *embedded approach*, shown to predict local

properties with good accuracy [45]. Here, a cell of 45 atoms containing one filler plus the cage atoms was treated at a quantum level. This cell was segregated by two atomic layers of atoms described as capped effective core potentials (cECPs) to avoid spurious electron leakage [45]. The remaining atoms were simulated in a molecular mechanics approach, with their charges ascribed in agreement with the Zintl phase concept to constrain the 24 electron rule per FeSb_3 unit [3] by means of a force field. All atomic positions were obtained from crystallographic data. For all atoms, the BP86 GGA functional was used along with the Karlsruhe valence triple ζ basis set with one set of polarization functions. Spin-orbit coupling effects were considered but no sizable effects were observed in the constitution of most relevant bonding MOs.

III. RESULTS AND DISCUSSION

A. EXAFS analysis and vibrational properties

Our EXAFS experiments focus on the Fe K -edge EXAFS of the $R\text{Fe}_4\text{Sb}_{12}$ ($R = \text{K}, \text{Ca}, \text{and Ba}$) materials to understand how their vibrational properties evolve as a function of the filler. Among the $R = \text{Na}, \text{K}, \text{Ca}, \text{Sr}, \text{and Ba}$ -filled materials, the changing periodic properties concern the filler charge and the filler-cage mass-size relation. By selecting the K- and Ca-filled materials, we probe the effects of the filler charge, whereas the filler-cage mass relation is kept nearly constant. Choosing the Ca- and Ba-filled cases, the filler-cage mass-size relation is probed, whereas the filler charge is kept constant. Our choice of R thus suffices to capture the important trends of the vibrational dynamics of the $R\text{Fe}_4\text{Sb}_{12}$ materials.

In Figs. 1(a)–1(c) we present three representations of the skutterudite structure. The R fillers, Fe atoms and Sb atoms are represented, respectively, by red, blue, and green spheres. In Fig. 1(a), we show the typical conventional unit-cell representation, where we highlight the FeSb_6 octahedra. In Fig. 1(b), we centered the representation in a given Fe atom, which we call the absorber, and leave only the atoms that are about 5 Å apart from this Fe atom. In Fig. 1(c), we show an alternative representation, where we show the filler, the square Sb ring, and the Fe cage. This representation highlights the vibrating components of the effective one-dimensional (1D) model for the correlated rattling dynamics in filled skutterudites [34,35] which we discuss below.

The Fourier-transformed data for all T values are presented in Figs. 1(d), 1(e), and 1(f) for the $R = \text{K}, \text{Ca}, \text{and Ba}$ materials, respectively. Our EXAFS analysis is based upon single- and multiple-scattering paths within the cluster depicted in Fig. 1(b). This cluster includes all atoms within 5 Å from the absorber. In this range, there are five Fe- Y single scattering paths, where Y is the scattering element. The second and third Sb nearest neighbors, denoted Sb_2 and Sb_3 , are too close to each other, and thus we adopt a single correlated Debye-Waller parameter $\sigma_{\text{Fe-Sb}_{2,3}}^2$ to describe both paths. In total, four $\sigma_{\text{Fe-Y}}^2$ are considered: $\sigma_{\text{Fe-Sb}_1}^2$, $\sigma_{\text{Fe-R}_1}^2$, $\sigma_{\text{Fe-Sb}_{2,3}}^2$, and $\sigma_{\text{Fe-Fe}_1}^2$. Single scattering paths dominate the EXAFS signal, but multiple-scattering paths were included to improve the data refinement. The disorder parameters of the latter were modeled in terms of the single scattering path $\sigma_{\text{Fe-Y}}^2$ parameters. In its turn, the T dependence of the $\sigma_{\text{Fe-Y}}^2$ parameters was

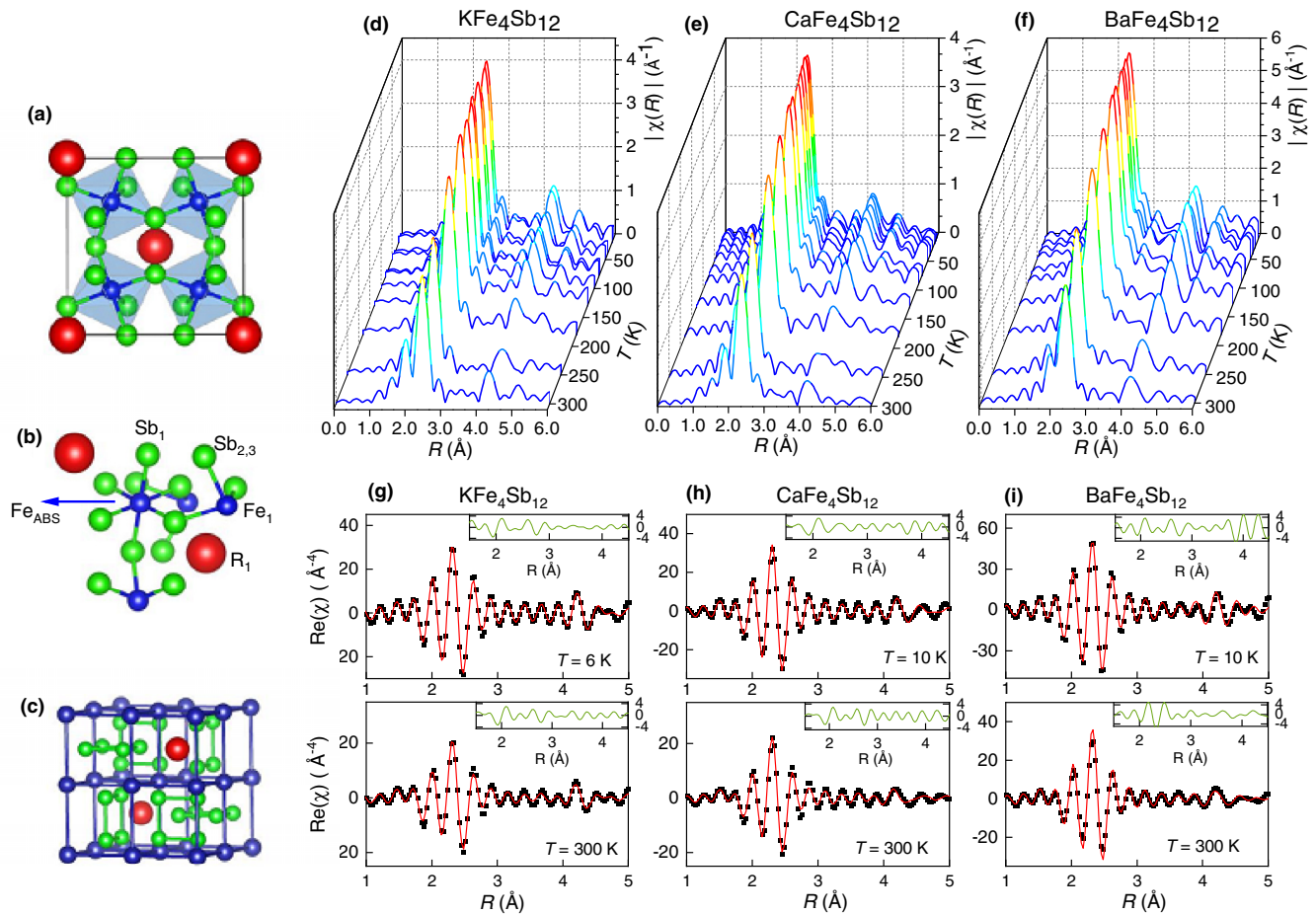


FIG. 1. (a)–(c) Three representations of the ternary filled skutterudite structure (space group $Im\bar{3}$): (a) the RFe_4Sb_{12} conventional unit-cell highlighting the $FeSb_3$ distorted octahedra; (b) the structural elements considered in the EXAFS analysis; (c) the vibrating elements of the 1D correlated rattling model (see text) [46]. In all cases, the R , Fe and Sb atoms are represented by, respectively, red, blue, and green spheres. (d)–(f) Fourier-transformed EXAFS spectra of the $R = K, Ca,$ and Ba materials in T -interval $6\text{ K} < T < 300\text{ K}$. (g)–(i) Low- T (upper panel) and high- T (lower panel) representative EXAFS data and data analysis (thick red line) for the $R = K, Ca,$ and Ba materials. In each panel, the inset shows the residuals of the presented fittings.

modeled on the basis of the Debye model for correlated disorder for all Fe- Y paths but the Fe- R paths, which were analyzed under the Einstein model, as typical for filled skutterudite materials [32,33]. Higher-order cumulants, which suggest the presence of anharmonic vibrations [47], were not adopted in our models. Representative fittings and residuals (for low- and high- T data) for the $R = K, Ca,$ and Ba cases are displayed in Figs. 1(g)–1(i), showing that the structural model adopted in this paper offers a fair description of the data in all T intervals.

In Figs. 2(a)–2(c) we show the correlated Debye-Waller parameters obtained from the EXAFS experiments. Whereas the Fe-Sb₁ and Fe-Sb_{2,3} bond disorder parameters are nearly R -independent, the difference between the Fe-Fe and Fe- R disorder parameters is significant when the cases of the light and heavy fillers are compared. This concerns not only the temperature dependence of the parameters, which is set by the relevant energy scales (either the Debye or Einstein temperatures), but also the order of magnitude of the parameters. In particular, one should note the relatively small disorder of the Fe-Ba path in comparison with the Fe-K and Fe-Ca

cases. For a more quantitative analysis, we turn to the obtained energy scales. From now on, we denote by $\theta_D^{R,Fe-Y}$ the Debye temperature obtained for the Fe- Y path of the R -filled sample and by θ_E^{Fe-R} the analogous Einstein temperature. All results are compiled in Table I.

The $\theta_D^{R,Fe-Sb_1}$ parameters display a weak dependence with R and compare well with those obtained in the early study by Cao *et al.* [32] for the $R = Ce$ and La cases ($\approx 390\text{ K}$), suggesting that the Fe-Sb bondings are not much affected by the filler. The θ_E^{Fe-R} here obtained, however, are significantly larger than those obtained by EXAFS of the $R = La$ and Ce cases but are closer to values determined from atomic displacement parameters (ADPs) for the $R = Ba$ and Ca cases by Schnelle *et al.* [15] (one should, of course, keep in mind the difference between the quantities obtained by EXAFS and ADPs). As for the overall trend in the data, $\theta_E^{Fe-Ba} > \theta_E^{Fe-K} > \theta_E^{Fe-Ca}$, similar results are obtained by heat capacity [15], even though the heat-capacity results are more indicative of $\theta_E^{Fe-Ba} > \theta_E^{Fe-K} \approx \theta_E^{Fe-Ca}$. Concerning the $\theta_D^{R,Fe-Fe}$ parameters, the values obtained in the $R = K$ or Ca cases are similar to results for other skutterudites [32,33,35] whereas

TABLE I. The θ (either $\theta_D^{R,Fe-Y}$ or θ_E^{Fe-R}) and K_{eff} parameters obtained from the analysis of the correlated Debye-Waller parameters.

Fe <i>K</i> -edge path	KFe ₄ Sb ₁₂		CaFe ₄ Sb ₁₂		BaFe ₄ Sb ₁₂	
	θ (K)	K_{eff} (eV/Å ²)	θ (K)	K_{eff} (eV/Å ²)	θ (K)	K_{eff} (eV/Å ²)
Fe-Sb ₁	422(15)	8.13	419(14)	8.13	426(17)	8.45
Fe- <i>R</i>	168(61)	1.15	134(51)	0.74	190(43)	2.55
Fe-Sb _{2,3}	356(26)	3.85	323(23)	3.12	360(15)	3.92
Fe-Fe ₁	395(75)	3.56	390(77)	3.45	620(80)	9.79

the Fe-Fe vibrations are particularly harder in the $R = \text{Ba}$ case.

The high-temperature limit of the σ^2 parameters of each single scattering path can be connected to an effective spring constant (K_{eff}) as discussed in detail in Refs. [33,35]. We denote by $K_{\text{eff}}^{R,Fe-Y}$ the effective spring constant for the Fe- Y path of the R -filled sample. Effective spring constants describe better the vibrational properties than a direct comparison between the Debye (Einstein) temperatures since they take into account the reduced mass of the vibrating elements and the fact that the $K_{\text{eff}}^{R,Fe-Y}$ are not linearly dependent on the Debye (Einstein) temperatures. The parameters are listed in Table I.

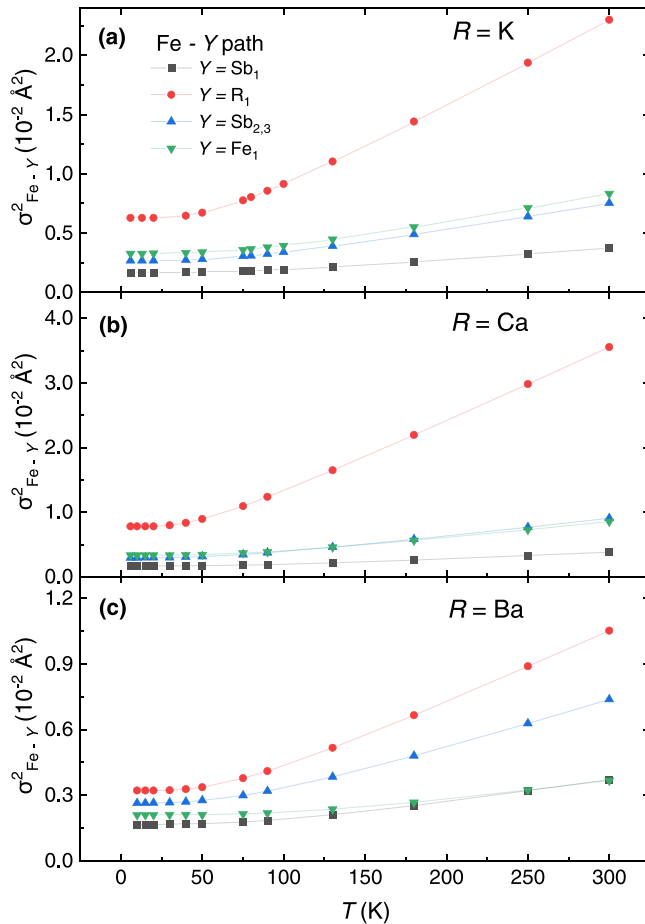


FIG. 2. Temperature dependence of the correlated Debye-Waller parameters obtained from the Fe *K*-edge EXAFS analysis for the (a) KFe₄Sb₁₂, (b) CaFe₄Sb₁₂, and (c) BaFe₄Sb₁₂ samples.

Translated to $K_{\text{eff}}^{R,Fe-Y}$, the vibrational properties of Fe-Sb bondings for the $R = \text{K}$ -, Ca -, and Ba -filled materials are similar, with the difference being less than 5% between the parameters $K_{\text{eff}}^{R,Fe-Sb_1}$. They are also very similar to the vibrational properties of the Co-Sb bondings as investigated by EXAFS [48]. Inspection of the $K_{\text{eff}}^{R,Fe-R}$ parameters, on the other hand, reveals a much larger variation as a function of R . Indeed, $K_{\text{eff}}^{\text{Ba,Fe-Ba}}/K_{\text{eff}}^{\text{Ca,Fe-Ca}} \approx 3.5$, stating a clear distinction between the cases of heavy and light fillers. It suggests a relative decoupling of the filler-cage vibrational dynamics in the case of the light-weight cations, a result that is in agreement with previous analysis of the $R\text{Fe}_4\text{Sb}_{12}$ atomic displacement parameters (ADPs) [15]. It so appears that the light-weight cations may behave as “rattlers” which, however, are not totally independent of the cage vibrations. We note that the $K_{\text{eff}}^{\text{Ba,Fe-Ba}}$ parameter compares well with the Ru-Ce and Pt-La cases, obtained from EXAFS experiments of CeRu₄As₁₂ [34,35] and LaPt₄Ge₁₂ [49], respectively, which are other examples of heavy-filler filled skutterudites. These results, however, are not simply expressing the filler-cage mass relation, but rather the potential energies of the cations, as discussed by previous calculations of $R\text{Fe}_4\text{Sb}_{12}$ [16]. The Fe-Fe vibrations are evinced by the analysis of the $K_{\text{eff}}^{R,Fe-Fe}$ parameters to be distinctively harder in the case of the Ba-filled samples, suggesting stronger Fe-Fe bonding in this case. We note that $K_{\text{eff}}^{\text{Ba,Fe-Fe}}/K_{\text{eff}}^{R,Fe-Fe} \approx 2.8$ for both $R = \text{K}$ or Ca .

The effective spring constants can be applied to the discussion of an effective 1D phonon model, introduced by Keiber *et al.* [33,35], for the qualitative description of the correlated filler-cage motion in filled skutterudites. The model considers the three distinct elements illustrated in Fig. 1(c): the R filler (or rattler), the Sb square ring, and the Fe metal cage, which denotes solely the Fe cubic lattice. The coupled character of the vibrational dynamics is given by connecting the elements by four distinct spring constants for each R -filled skutterudite: a rattler-square ring (k_{rs}^R), a rattler-metal cage (k_{rc}^R), a metal cage-metal cage (k_{cc}^R), and a metal cage-square ring (k_{cs}^R). The system dynamics is treated at a classical level and the corresponding dynamic matrix is diagonalized to find four phonon dispersion modes $\omega_j(q)$, where q is the phonon wave vector [35]. We discuss two aspects of the coupled vibrations that can be connected to our experimental results: (i) the filler-cage mass relation, and (ii) the dependence of the k_{rc}^R constants on whether R is a light or heavy element (as suggested by the experimentally obtained $K_{\text{eff}}^{R,Fe-R}$ parameters). Moreover, we fix the parameter $k_{\text{cs}}^R = 1.8 \text{ eV}/\text{\AA}^2$ for all samples, as suggested by the experimentally obtained $K_{\text{eff}}^{R,Fe-Sb}$ and adopt $k_{\text{cc}}^{\text{K(Ca)}} = 10$

$eV/\text{\AA}^2$ and $k_{cc}^{\text{Ba}} = 25 \text{ eV}/\text{\AA}^2$ based on the variation of the obtained $K_{\text{eff}}^{R,\text{Fe-Fe}}$ parameters. Our experiments do not offer an estimate about the k_{rs}^R parameters and we chose to adopt a range of values in reference to previous works [34,35].

One should keep in mind that there is no one-to-one correspondence between the $K_{\text{eff}}^{R,\text{Fe-Y}}$ and spring constants of the 1D effective model. Rather, the $K_{\text{eff}}^{R,\text{Fe-Y}}$ constants are adopted to get reasonable estimates to the spring constants, in particular to their relative values. Formally, the spring constants are a functional of the $K_{\text{eff}}^{R,\text{Fe-Y}}$ and there is a strong functional dependence between, for instance, $K_{\text{eff}}^{R,\text{Fe-Fe}}$ and k_{cc}^R or $K_{\text{eff}}^{R,\text{Fe-R}}$ and k_{rc}^R . Results of the phonon dispersion and the exact parameters adopted are displayed in Figs. 3(a)–3(o) and in the figure caption.

In Figs. 3(a)–3(i), the mass relation between the R cations and the cage elements is that of the $\text{KFe}_4\text{Sb}_{12}$ case (which, in view of the qualitative nature of the calculated dispersions, also describe the $\text{CaFe}_4\text{Sb}_{12}$ case) and is one of the key properties determining the phonon dispersion. The other relevant parameter is indeed the relatively small rattler-cage spring constant. These two parameters determine, respectively, the wide separation between the acoustic and optical modes and the conspicuous flattening of the second optical mode (thick orange line). The latter implies a wide range of q values for which the phonon group velocity is very close to zero, describing a rather localized phonon mode, reminiscent of the Einstein oscillators scenario. In view of the ratio $K_{\text{eff}}^{\text{Ca,Fe-Ca}}/K_{\text{eff}}^{\text{K,Fe-K}} \approx 2/3$ (see Table I) we propose that the $\text{CaFe}_4\text{Sb}_{12}$ and $\text{KFe}_4\text{Sb}_{12}$ vibrational dynamics are, respectively, described by Figs. 3(a)–3(c) and 3(g)–3(i). The range of values in the k_{rs}^R leaves the acoustic and first optical modes unchanged (red and green lines), while pushing the second optical mode (orange) up, causing this mode to interact with the third one (blue).

The mass relation of the $\text{BaFe}_4\text{Sb}_{12}$ case is represented in Figs. 3(j)–3(o). We now observe a smaller frequency gap between the acoustic and optical modes (due to the filler-cage mass relation) and a much smaller region wherein the second optical mode is flat, due to the large rattler-cage coupling. Here, the parameters' range is similar to the one adopted in the $\text{CeRu}_4\text{As}_{12}$ [35] and $\text{LaPt}_4\text{Ge}_{12}$ [49] cases, which allows us to pinpoint that the filler-cage mass relation is also responsible for a larger flattening of the optical mode, contributing to the phonon localization as recently proposed [50]. The value of the k_{cc}^{Ba} constant (reflecting the large $K_{\text{eff}}^{\text{Ba,Fe-Fe}}$) is twice the value for the other heavy-filler filled skutterudites and it essentially increases the frequency of the higher energy (blue) optical mode. In comparison to the K (Ca) case, this shift of the third optical mode to a higher frequency causes the decoupling of this mode from the second optical mode, which in the Ba case turns out to interact mainly with the first optical mode.

B. X-ray diffraction and elastic properties

We now turn to the P -dependent XRD experiments. In Figs. 4(a)–4(e) representative data of the XRD experiments, after removing the background, are presented for all samples. The main diffraction peaks of the skutterudite structure are

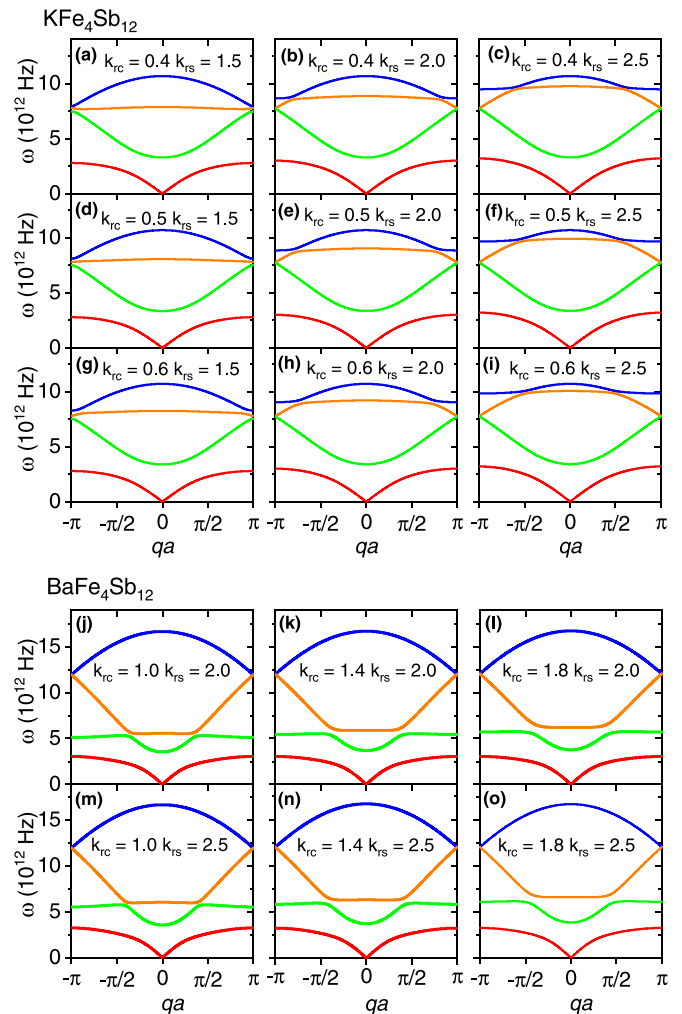


FIG. 3. Effective 1D correlated rattling model for the $R = \text{K}$ (Ca) and Ba samples. In ascending frequency, we have the acoustic mode (red) and the first, (green), second (orange), and third (blue) optical phonon modes. The modes are displayed as function of qa where a is the material lattice constant and q is the phonon wave vector. In panels (a)–(i), the mass relation between the vibrating elements is that of the $R = \text{K}$ case and, in panels (j)–(o), the mass relation between the vibrating elements is that of the $R = \text{Ba}$ case. The adopted parameters are $k_{cs}^R = 1.8 \text{ eV}/\text{\AA}^2$ for all panels and $k_{cc}^{\text{K}} = 10 \text{ eV}/\text{\AA}^2$, in panels (a)–(i), and $k_{cc}^{\text{Ba}} = 25 \text{ eV}/\text{\AA}^2$, in panels (j)–(o), reflecting the different $K_{\text{eff}}^{R,\text{Fe-Fe}}$ parameters. The adopted k_{rs}^R and k_{rc}^R values are indicated in each panel in units of $\text{eV}/\text{\AA}^2$.

marked in red as a reference. The powder profile was compared with the skutterudite crystal structure [the thick red lines in Figs. 4(a)–4(e)] and the P dependence of the lattice parameters was extracted from the peak positions. The blue and green arrows point to peaks that are not part of the skutterudite phase. The peaks are, respectively, ascribed to small amounts of nonreacted Sb and to the sample decomposition at high P [51].

Our analysis of the XRD experiments are in Figs. 5(a)–5(d). In Fig. 5(a), the unit-cell volumes (V) as a function of P of all samples are presented. It is tempting to associate the skutterudite elastic properties to the relation between the cage volume and the filler cationic size. We then compile in

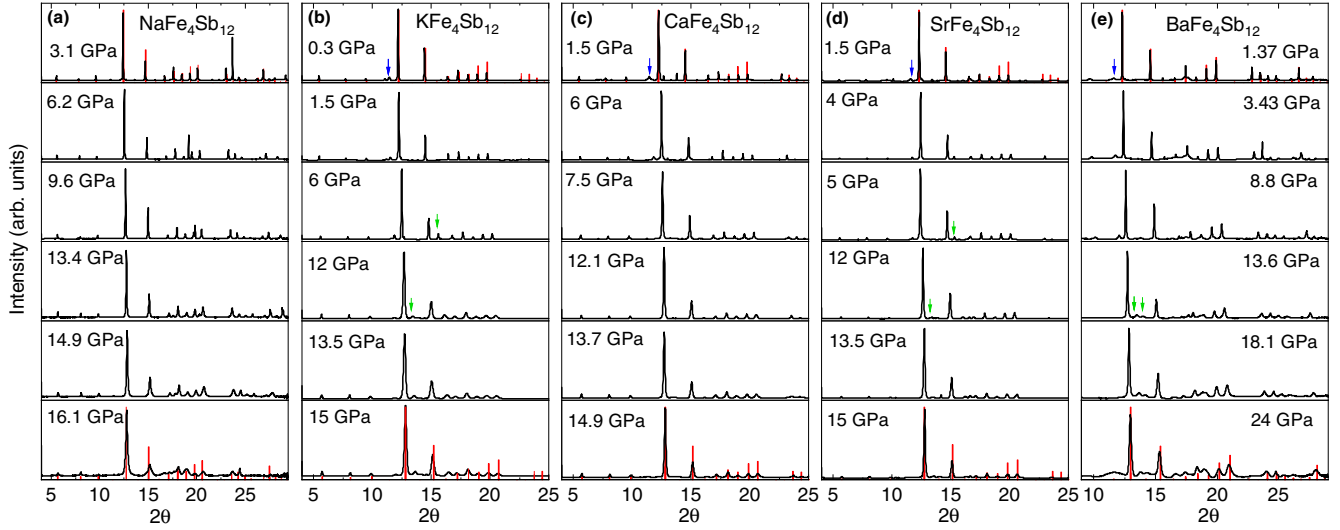


FIG. 4. Representative P dependent XRD experiments for all $R\text{Fe}_4\text{Sb}_{12}$ -filled skutterudite, wherein we have (a) $R = \text{Na}$, (b) $R = \text{K}$, (c) $R = \text{Ca}$, (d) $R = \text{Sr}$, and (e) $R = \text{Ba}$. P is as indicated in the panels. The thick red lines represent the diffraction peaks of the skutterudite structure. The blue and green arrows point to diffraction peaks not ascribed to the skutterudite phase and are discussed in the main text and elsewhere [51].

Fig. 5(b) a phenomenological parameter: the cage empty volume fraction f_E , which we define as $f_E = 1 - V_R/V_C$, where V_R is the R cationic volume and V_C is the Sb cage volume, as a function of P . The cage is represented in the inset of Fig. 5(b) as a reference.

The volume pressure dependence is investigated by fitting $V \times P$ data to the Birch-Murnaghan (BM) model [36]:

$$P(V) = \frac{3}{2}B_0 \left[\left(\frac{V}{V_0} \right)^{-\frac{7}{3}} - \left(\frac{V}{V_0} \right)^{-\frac{5}{3}} \right] \times \left\{ 1 + \frac{3}{4} \left(B'_0 - 4 \right) \left[\left(\frac{V}{V_0} \right)^{-\frac{2}{3}} - 1 \right] \right\}, \quad (1)$$

where V is the sample unit-cell volume, V_0 is the sample volume at room conditions, B_0 is the bulk modulus, and B'_0 is the bulk modulus derivative. We keep $B'_0 = 4$ GPa, as recently adopted to describe other skutterudites [52,53] in this pressure range. Values obtained for V_0 and B_0 are compiled in Table II. The V_0 values obtained from the fitting deviate only about 1% from the experimentally determined from x-ray diffraction at room conditions suggesting the adequacy of our analysis. The $V \times P$ data and their respective fittings are in Fig. 5(c).

The B_0 values thus obtained range from 77 GPa ($R = \text{K}$) to 99 GPa ($R = \text{Ba}$). The values compare well with those obtained for other $R\text{Fe}_4\text{Sb}_{12}$ -based skutterudites, such as $\text{EuFe}_4\text{Sb}_{12}$ [52] and $\text{CeFe}_4\text{Sb}_{12}$ [54,55]. The latter further

TABLE II. Parameters of the Birch-Murnaghan model for all $R\text{Fe}_4\text{Sb}_{12}$ samples.

$R =$	Na	K	Ca	Sr	Ba
$V_0(\text{\AA}^3)$	768.3(7)	787.8(2)	778.7(5)	777.6(5)	772.0(3)
$B_0(\text{GPa})$	94(7)	77(5)	87(6)	91(6)	99(3)

suggests that B_0 reflects the rigidity of the $\text{Fe}_4\text{Sb}_{12}$ framework which, however, is not in total R independent. The experimentally obtained B_0 parameters are in the range of the values previously obtained by calculations of the $R = \text{Ca}$, Sr , and Ba cases [17]. It is noteworthy, however, that the calculated values are nearly R independent and about 80 GPa. Our results also compare well with other Sb-based skutterudites, such as CoSb_3 [53], in agreement with the understanding that the pnictogen square ring rigidity dominates the skutterudite elastic properties. Indeed, the wider variation in B_0 is observed when the pnictogen is changed, with P forming characteristically rigid cages [54].

In possession of the B_0 values, we then obtain the materials' compressibility β as a function of P . The results are displayed in Fig. 5(d). The compressibility data express well how the elastic properties depend on R : it is shown that the K- and Ca-filled materials have larger β while the Ba- and Na-filled materials have smaller β . It is a natural assumption to speculate that the higher f_E more compressible would be the material. If the whole data are inspected, this trend is not obeyed. For instance, the Ca-filled material, which has the largest f_E , is not the most compressible. If, however, we focus on either the R^{1+} - or R^{2+} -filled materials, an interesting picture emerges. Restricting the analysis to the case of the R^{1+} fillers, one notes that this simple picture does not work and β does not correlate with f_E , with the K-filled material being the more compressible. Now, if one inspects the case R^{2+} -filler case, the experimentally obtained picture obeys the proposed trend, with the Ca-filled material being the more compressible.

The case of the alkaline-earth-filled materials is distinct due to the presence of the heavy Sr and Ba fillers. Here, Sr and Ba virtual atomic $4d$ and $5d$ states, respectively, are more extended in real space as well as energetically accessible than in the case of the Ca virtual $3d$ states. Thus, the $4d$

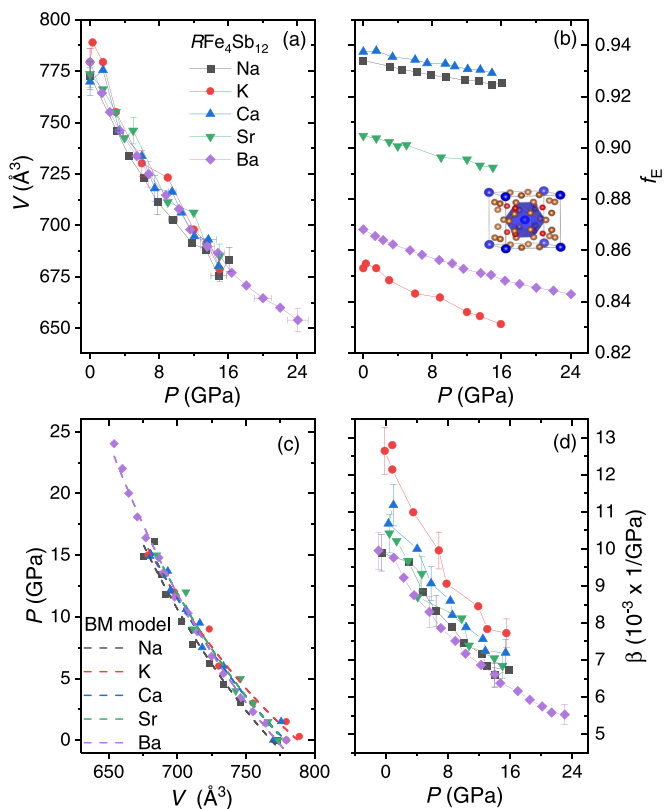


FIG. 5. (a) The unit-cell volume V as function of P . Error bars for P are estimated from the half-width at half maximum of the ruby fluorescence spectra and amount to about 3%–5 % in this pressure interval. (b) The cage empty volume fraction f_E (see text) as a function of P . The inset shows a representation of the skutterudite structure highlighting the Sb cage around the filler site (the cage volume was calculated with VESTA [46]). (c) The P as a function of V data and their respective fittings to the Birch-Murnaghan model. (d) The compressibility β as a function of P for all samples.

and $5d$ states may take part in the filler-cage bonding which, in this scenario, is not completely ionic in character, as has been proposed for La-filled skutterudites [56]. To verify this hypothesis, we performed DFT calculations of the filler-cage bonding properties.

We focus our analysis on the DFT results on the filler-derived atomic orbital (AO) contribution to the molecular orbitals (MOs) with the highest superposition with the Sb-derived $5p$ states, since these are precisely the MOs contributing the most to the filler-cage bonding. These MOs sit in the vicinity of the Fermi Level (see Ref. [51]). Our results

show that, whereas the $4d$ and $5d$ virtual AOs from Sr and Ba, respectively, take part in the formation of these MOs, Ca only contributes its $3p$ states to the bonding MOs. In Table III, we list the filler-derived AOs contributing the most (largest superposing orbitals) to the formation of the filler-cage bonding MOs. The MO symmetry classification is indicated and is made in terms of the irreducible representations of the T_h group, which is the point-group symmetry of the R site [57,58]. The results were obtained at room conditions and at high P (≈ 13.6 GPa). The P effect was simulated by adopting the results from our XRD experiments.

As can be observed, pressure has nearly no effect on the bonding in the case of the Ca filler, whereas it further stabilizes and increases the d states participation in the Sr- and Ba-filled materials. This effect is particularly large in the case of Ba, for which an increase of $\gtrsim 40\%$ of the $5d$ orbital contribution to MOs enrolled in the filler-cage bonding is observed in high- P calculations. This result means that, on top of geometrical considerations, one must consider that P induces further stabilization to the filler-cage bonding via the available virtual nd states, rendering the material more rigid. Our findings thus suggest that the association between B_0 (or β) and f_E in the case of the R^{2+} fillers actually reflects a deeper understanding of the problem based upon the filler-cage bonding properties, particularly in the case of the heavy fillers. This mechanism could also be at work in the context of the partially filled $M_y\text{Co}_4\text{Sb}_{12}$ skutterudites, for which it is observed that, when M is a heavy filler, particularly in the cases of $M = \text{La}$ and Yb , the material is more rigid [53]. Moreover, our calculations suggest an association between the participation of the Ba $5d$ states in the filler-cage bonding and the relatively large value of the $K_{\text{eff}}^{\text{Fe-Ba}}$ parameter.

A better visualization of the filler-cage bonding, in particular of the d character of the MOs in the Sr and Ba case, can be observed in Fig. 6, wherein we depict the MOs related to the results listed in Table III. The plots are contour plots of the mentioned MOs and illustrate the real space electron density distribution around the filler atom, which is located at the center of the figures. As is clear, the plotted MOs are dominated by orbitals of d character in the case of Sr- and Ba-filled materials, whereas in the case of Ca-filled material the presence of the $3p$ lobe dominating the MOs is clearly distinguishable.

Lastly, we comment on the significant broadening of the diffraction peaks for high pressures that is observed. Starting at about 12 GPa in the $R = \text{Na}$ and K cases and at higher P in the case of the alkaline-earth-filled skutterudites, the peaks' broadening amounts to an increasing structural

TABLE III. The highest filler derived superposing AOs to the formation of the MOs connected to the filler-cage bonding. The nature of the AOs and the symmetry character of the MOs are indicated. The final orbital composition analysis was performed adopting the Ros-Schuit partition method via the MULTIFWN program [59].

R	AO character	Room pressure		≈ 13.6 GPa	
		Orbital cont. (%)	$E - E_F$ (eV)	Orbital cont. (%)	$E - E_F$ (eV)
Ca	$3p_x (t_u)$	30.77	−3.23	30.82	−3.46
Sr	$4d_{xy}, 4d_{xz}, 4d_{yz} (t_g)$	11.84	−1.70	15.37	−1.82
Ba	$5d_{xy}, 5d_{xz}, 5d_{yz} (t_g)$	19.54	−1.60	28.00	−1.68

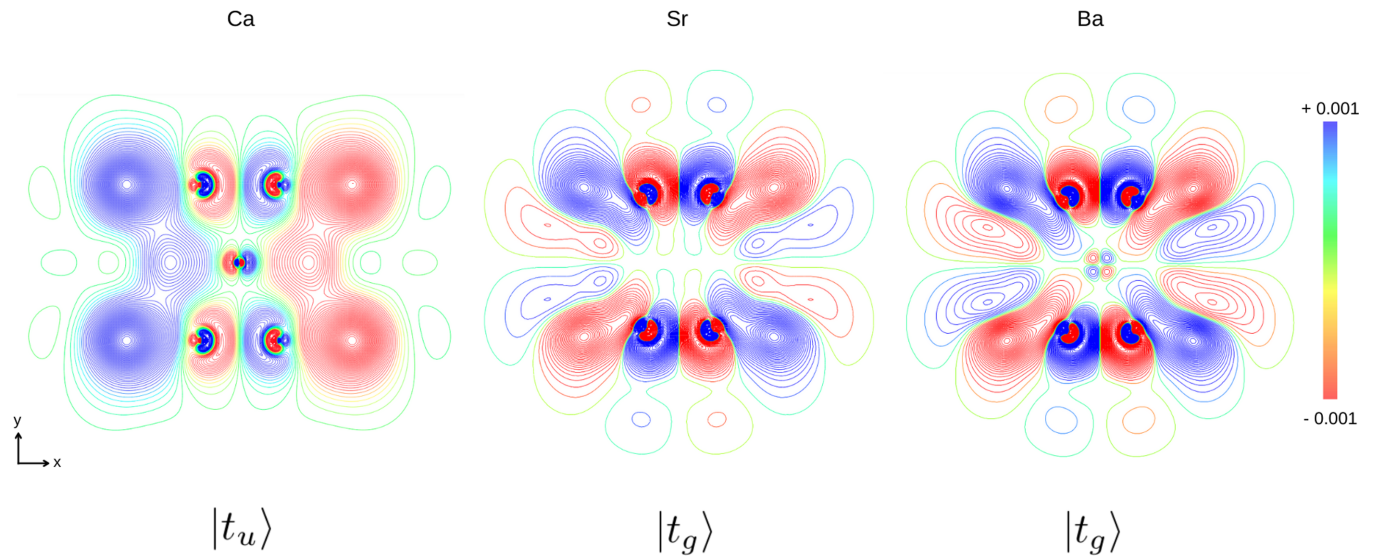


FIG. 6. Contour plots for the MOs describing the filler-cage bonding in the (x, y) plane in the cases of the Ca-, Sr-, and Ba-filled materials as indicated. The figures are formed by 120 contours in the isovalue interval indicated in the color scale on the right side of the figure. Ligand orbitals are plotted via the GABEDIT program [60].

disorder induced by P . The alkaline-earth-filled materials are suggested to be relatively less susceptible to the disorder increase by P . Indeed, the diffraction peaks can still be observed for P up to 24 GPa in the $\text{BaFe}_4\text{Sb}_{12}$ case. The skutterudite structure is mainly stabilized by a combination of geometric and charge constraints related to the filler and cage sizes and charge distribution [2,3]. We thus conclude that the larger structural stability of alkaline-earth-filled materials is likely due to the bonding stabilization of the extra charge offered by the R^{2+} cations.

IV. SUMMARY AND CONCLUSIONS

The site specific vibrational properties of the $R = \text{K}$ -, Ca-, and Ba-filled skutterudites $R\text{Fe}_4\text{Sb}_{12}$ were investigated by EXAFS experiments. As concluded from the effective spring constants obtained from experiments, materials filled with light-weight cations display weak rattler-cage couplings, reminiscent of the independent rattler scenario, and the $R = \text{Ba}$ material displays a characteristic strong Fe-Fe coupling. Based upon an effective 1D model for the skutterudite phonon dispersion, we proposed that the $R = \text{K}$ - and Ca-filled skutterudites should display a conspicuous optical flat mode in accordance with the Einstein oscillator scenario.

We thus introduced our pressure-dependent experiments. The $V \times P$ curves were determined and fit to the Birch-Murnaghan model to extract the bulk modulus B_0 and then the compressibility β . We found that the geometric parameter f_E cannot explain the B_0 (or β) dependence as a function of R . A geometrical relation, however, was observed to hold in the case of the R^{2+} filled materials. By considering DFT calculations, we uncovered that this association between B_0

(or β) and f_E actually reflects an emerging property of the filler-cage bonding, which is particularly relevant for heavy fillers. Moreover, the filler-cage bonding can also explain the large $K_{\text{eff}}^{\text{Fe-Ba}}$ parameter, since the contribution from Ba $5d$ states to bonding makes the Ba more tightly coupled to the cage (no “independent” rattler in this case).

From the point of view of material design, our results suggest that synthesizing mixed filled skutterudites, featuring light and heavy fillers, is a good strategy to introduce localized vibrational modes (“rattlers”) in the material’s vibrational dynamics. This speculation has some ground on our calculations showing that the bonding scheme in skutterudites may include a certain degree of covalency in the case of heavy fillers. Thus, introducing light cations into materials mainly filled with heavy cations create a situation wherein the light fillers are weakly bonded and sitting in an oversized cage.

ACKNOWLEDGMENTS

The authors acknowledge CNPEM-LNLS for the concession of beam time (Proposals No. 20160180, No. 20160181, No. 20170709 and No. 20190018). The XAFS2 and XDS beamlines staff are acknowledged for the assistance during the experiments. A.L.-J. thanks J. Grin for his steady support and interest in this work. The Fundação de Amparo à Pesquisa do Estado de São Paulo financial support is acknowledged by M.R.C. (Grant No. 2019/05150-7 and Grant No. 2020/13701-0) and F.A.G. (Grant No. 2019/25665-1). This study was financed in part by CAPES - Finance Code 001. E.M.B. acknowledges Fundação Carlos Chagas Filho de Amparo à Pesquisa do Estado do Rio de Janeiro (Grant No. E-26/202.798/2019).

[1] W. Jeitschko and D. Braun, *Acta Crystallogr., Sect. B: Struct. Crystallogr. Cryst. Chem.* **33**, 3401 (1977).

[2] R. Gumenuik, H. Borrmann, A. Ormeci, H. Rosner, W. Schnelle, M. Nicklas, Y. Grin, and A. Leithe-Jasper, *Z. Kristallogr. - Cryst. Mater.* **225**, 531 (2010).

- [3] H. Luo, J. W. Krizan, L. Muechler, N. Haldolaarachchige, T. Klimczuk, W. Xie, M. K. Fuccillo, C. Felser, and R. J. Cava, *Nat. Commun.* **6**, 6489 (2015).
- [4] V. Keppens, D. Mandrus, B. C. Sales, B. C. Chakoumakos, P. Dai, R. Coldea, M. B. Maple, D. A. Gajewski, E. J. Freeman, and S. Bennington, *Nature (London)* **395**, 876 (1998).
- [5] G. J. Snyder and E. S. Toberer, *Nat. Mater.* **7**, 105 (2008).
- [6] J. Mao, Z. Liu, J. Zhou, H. Zhu, Q. Zhang, G. Chen, and Z. Ren, *Adv. Phys.* **67**, 69 (2018).
- [7] S. El Oualid, I. Kogut, M. Benyahia, E. Geczi, U. Kruck, F. Kosior, P. Masschelein, C. Candolfi, A. Dauscher, J. D. Koenig, A. Jacquot, T. Caillat, E. Alleno, and B. Lenoir, *Adv. Energy Mater.* **11**, 2100580 (2021).
- [8] R. P. Hermann, F. Grandjean, and G. J. Long, *Am. J. Phys.* **73**, 110 (2005).
- [9] F. A. Garcia, D. J. Garcia, M. A. Avila, J. M. Vargas, P. G. Pagliuso, C. Rettori, M. C. G. Passeggi, S. B. Oseroff, P. Schlottmann, B. Alascio, and Z. Fisk, *Phys. Rev. B* **80**, 052401 (2009).
- [10] F. A. Garcia, R. Gumenuik, W. Schnelle, J. Sichelschmidt, A. Leithe-Jasper, Y. Grin, and F. Steglich, *Phys. Rev. B* **85**, 134402 (2012).
- [11] M. M. Koza, M. R. Johnson, R. Viennois, H. Mutka, L. Girard, and D. Ravot, *Nat. Mater.* **7**, 805 (2008).
- [12] R. Wei, G. Huiyuan, Z. Zihao, and Z. Lixia, *Phys. Rev. Lett.* **118**, 245901 (2017).
- [13] W. Zhao, P. Wei, Q. Zhang, H. Peng, W. Zhu, D. Tang, J. Yu, H. Zhou, Z. Liu, X. Mu, D. He, J. Li, C. Wang, X. Tang, and J. Yang, *Nat. Commun.* **6**, 6197 (2015).
- [14] J. Gainza, F. Serrano-Sanchez, J. E. Rodrigues, J. Prado-Gonjal, N. M. Nemes, N. Biskup, O. J. Dura, J. L. Martinez, F. Fauth, and J. A. Alonso, *Adv. Funct. Mater.* **30**, 2001651 (2020).
- [15] W. Schnelle, A. Leithe-Jasper, H. Rosner, R. Cardoso-Gil, R. Gumenuik, D. Trots, J. A. Mydosh, and Y. Grin, *Phys. Rev. B* **77**, 094421 (2008).
- [16] M. M. Koza, L. Capogna, A. Leithe-Jasper, H. Rosner, W. Schnelle, H. Mutka, M. R. Johnson, C. Ritter, and Y. Grin, *Phys. Rev. B* **81**, 174302 (2010).
- [17] M. M. Koza, A. Leithe-Jasper, H. Rosner, W. Schnelle, H. Mutka, M. R. Johnson, M. Krisch, L. Capogna, and Y. Grin, *Phys. Rev. B* **84**, 014306 (2011).
- [18] J. L. Feldman, D. J. Singh, and N. Bernstein, *Phys. Rev. B* **89**, 224304 (2014).
- [19] A. Möchel, I. Sergueev, N. Nguyen, G. J. Long, F. Grandjean, D. C. Johnson, and R. P. Hermann, *Phys. Rev. B* **84**, 064302 (2011).
- [20] M. M. Koza, M. Boehm, E. Sischka, W. Schnelle, H. Mutka, and A. Leithe-Jasper, *Phys. Rev. B* **91**, 014305 (2015).
- [21] J. Prado-Gonjal, F. Serrano-Sanchez, N. M. Nemes, O. J. Dura, J. L. Martinez, M. T. Fernandez-Diaz, F. Fauth, and J. A. Alonso, *Appl. Phys. Lett.* **111**, 083902 (2017).
- [22] S. H. Bae, K. H. Lee, and S.-M. Choi, *Intermetallics* **105**, 44 (2019).
- [23] Y. Wang, J. Mao, Q. Jie, B. Ge, and Z. Ren, *Appl. Phys. Lett.* **110**, 163901 (2017).
- [24] M. B. Maple, R. E. Baumbach, J. J. Hamlin, D. A. Zocco, B. J. Taylor, N. P. Butch, J. R. Jeffries, S. T. Weir, B. C. Sales, D. Mandrus, M. A. McGuire, A. S. Sefat, R. Jin, Y. K. Vohra, J. H. Chu, and I. R. Fisher, *Phys. B (Amsterdam, Neth.)* **404**, 2924 (2009).
- [25] A. Leithe-Jasper, W. Schnelle, H. Rosner, N. Senthilkumaran, A. Rabis, M. Baenitz, A. Gippius, E. Morozova, J. A. Mydosh, and Y. Grin, *Phys. Rev. Lett.* **91**, 037208 (2003).
- [26] A. Leithe-Jasper, W. Schnelle, H. Rosner, M. Baenitz, A. Rabis, A. A. Gippius, E. N. Morozova, H. Borrmann, U. Burkhardt, R. Ramlau, U. Schwarz, J. A. Mydosh, Y. Grin, V. Ksenofontov, and S. Reiman, *Phys. Rev. B* **70**, 214418 (2004).
- [27] D. Berardan, E. Alleno, and C. Godart, *J. Magn. Magn. Mater.* **285**, 245 (2005).
- [28] E. Matsuo, K. Hayashi, A. Ikeda, K. Tanaka, T. Takabatake, and M. Matsumura, *J. Phys. Soc. Jpn.* **74**, 1382 (2005).
- [29] A. Leithe-Jasper, W. Schnelle, H. Rosner, W. Schweika, and O. Isnard, *Phys. Rev. B* **90**, 144416 (2014).
- [30] S.-i. Kimura, H. Im, T. Mizuno, S. Narazu, E. Matsuo, and T. Takabatake, *Phys. Rev. B* **75**, 245106 (2007).
- [31] B. Mounsséf, M. R. Cantarino, E. M. Bittar, T. M. Germano, A. Leithe-Jasper, and F. A. Garcia, *Phys. Rev. B* **99**, 035152 (2019).
- [32] D. Cao, F. Bridges, P. Chesler, S. Bushart, E. D. Bauer, and M. B. Maple, *Phys. Rev. B* **70**, 094109 (2004).
- [33] F. Bridges, B. Car, L. Sutton, M. Hoffman-Stapleton, T. Keiber, R. E. Baumbach, M. B. Maple, Z. Henkie, and R. Wawryk, *Phys. Rev. B* **91**, 014109 (2015).
- [34] F. Bridges, *Mod. Phys. Lett. B* **30**, 1630001 (2016).
- [35] T. Keiber and F. Bridges, *Phys. Rev. B* **92**, 134111 (2015).
- [36] F. Birch, *Phys. Rev.* **71**, 809 (1947).
- [37] J. R. L. Mardegan, G. Fabbris, L. S. I. Veiga, C. Adriano, M. A. Avila, D. Haskel, and C. Giles, *Phys. Rev. B* **88**, 144105 (2013).
- [38] S. J. A. Figueroa, J. C. Mauricio, J. Murari, D. B. Beniz, J. R. Piton, H. H. Slepicka, M. F. a. d. Sousa, A. M. Espíndola, and A. P. S. Levinsky, *J. Phys.: Conf. Ser.* **712**, 012022 (2016).
- [39] J. J. Rehr and R. C. Albers, *Rev. Mod. Phys.* **72**, 621 (2000).
- [40] B. Ravel and M. Newville, *J. Synchrotron Radiat.* **12**, 537 (2005).
- [41] F. A. Lima, M. E. Saleta, R. J. S. Pagliuca, M. A. Eleotério, R. D. Reis, J. Fonseca Júnior, B. Meyer, E. M. Bittar, N. M. Souza-Neto, and E. Granado, *J. Synchrotron Radiat.* **23**, 1538 (2016).
- [42] B. H. Toby and R. B. Von Dreele, *J. Appl. Crystallogr.* **46**, 544 (2013).
- [43] F. Neese, F. Wennmohs, U. Becker, and C. Riplinger, *J. Chem. Phys.* **152**, 224108 (2020).
- [44] F. Neese, *Wiley Interdiscip. Rev. Comput. Mol. Sci.* **2**, 73 (2012).
- [45] A. Dittmer, R. Izsák, F. Neese, and D. Maganas, *Inorg. Chem. (Washington, DC, US)* **58**, 9303 (2019).
- [46] K. Momma and F. Izumi, *J. Appl. Crystallogr.* **41**, 653 (2008).
- [47] Y. Hu, J. R. Salvador, N. Chen, A. Alatas, and Y.-J. Kim, *J. Appl. Phys.* **130**, 185105 (2021).
- [48] J. E. F. S. Rodrigues, J. Gainza, F. Serrano-Sánchez, C. Marini, Y. Huttel, N. M. Nemes, J. L. Martínez, and J. A. Alonso, *Chem. Mater.* **34**, 1213 (2022).
- [49] M. R. Cantarino, R. Lora-Serrano, R. Gumenuik, W. Schnelle, J. Sichelschmidt, A. Leithe-Jasper, Y. Grin, and F. A. Garcia (unpublished).
- [50] A. Valério, R. F. S. Penacchio, M. B. Estradiote, M. R. Cantarino, F. A. Garcia, S. L. Morelhão, N. Rafter, S. W. Kycia,

- G. A. Calligaris, and C. M. R. Remédios, *MRS Commun.* **10**, 265 (2020).
- [51] See Supplemental Material at <http://link.aps.org/supplemental/10.1103/PhysRevMaterials.6.085403> for powder x-ray diffraction data and details of the quantum chemistry calculations.
- [52] I. Sergueev, K. Glazyrin, I. Kantor, M. A. McGuire, A. I. Chumakov, B. Klobes, B. C. Sales, and R. P. Hermann, *Phys. Rev. B* **91**, 224304 (2015).
- [53] J. a. E. F. S. Rodrigues, J. Gainza, F. Serrano-Sánchez, M. M. Ferrer, G. S. L. Fabris, J. R. Sambrano, N. M. Nemes, J. L. Martínez, C. Popescu, and J. A. Alonso, *Inorg. Chem. (Washington, DC, US)* **60**, 7413 (2021).
- [54] I. Shirovani, T. Noro, J. Hayashi, C. Sekine, R. Giri, and T. Kikegawa, *J. Phys.: Condens. Matter* **16**, 7853 (2004).
- [55] W. Liu, Q. Jie, Q. Li, Z. Chen, and B. Li, *Phys. B (Amsterdam, Neth.)* **406**, 52 (2011).
- [56] A. P. Grosvenor, R. G. Cavell, and A. Mar, *Phys. Rev. B* **74**, 125102 (2006).
- [57] K. Takegahara, H. Harima, and A. Yanase, *J. Phys. Soc. Jpn.* **70**, 1190 (2001).
- [58] D. J. Garcia, F. A. Garcia, J. G. S. Duque, P. G. Pagliuso, C. Rettori, P. Schlottmann, M. S. Torikachvili, and S. B. Oseroff, *Phys. Rev. B* **78**, 174428 (2008).
- [59] T. Lu and F. Chen, *J. Comput. Chem.* **33**, 580 (2012).
- [60] A.-R. Allouche, *J. Comput. Chem.* **32**, 174 (2011).